Integration of rate and temporal codes by hippocampal cell-assemblies supports theta phase coding of episodic information

Eleonora Russo[1,2*], Nadine Becker[3,4], Aleks P. F. Domanski[3], Daniel Durstewitz[2,5], Matthew W. Jones[3,5]

[1] Department of Psychiatry and Psychotherapy, University Medical Center, Johannes Gutenberg University, 55131 Mainz, Germany.
[2] Dept. of Theoretical Neuroscience, Central Institute of Mental Health, Medical Faculty Mannheim, Heidelberg University, 68159 Mannheim, Germany.
[3] School of Physiology, Pharmacology & Neuroscience, Faculty of Life Sciences, University of Bristol, University Walk, Bristol BS8 1TD, UK.
[4] Current address: Nanion Technologies GmbH, Ganghoferstr. 70A, D-80339 Munich – Germany.
[5] Equal contribution.
* Corresponding author, email: eleonora.russo@zi-mannheim.de

Abstract

Spatial information is encoded by location-dependent hippocampal place cell firing rates and sub-second, rhythmic modulation of spike times. These 'rate' and 'temporal' codes have primarily been characterized in low-dimensional environments under limited cognitive demands; but how is coding configured in complex environments when individual place cells signal several locations, individual locations contribute to multiple routes and functional demands vary? Quantifying rat CA1 population dynamics during a decision-making task, we show that the phase of individual place cells' spikes relative to the local theta rhythm shifts to differentiate activity in different place fields. Theta phase coding also disambiguates repeated visits to the same location during different routes, particularly preceding spatial decisions. Using unsupervised detection of cell assemblies alongside theoretical simulation, we show that integrating rate and phase coding mechanisms dynamically recruits units to different assemblies, generating spiking sequences that disambiguate episodes of experience and multiplexing spatial information with cognitive context.

Keywords: cell assemblies, precession, temporal coding, rate coding, CA1, theta phase, theta sequences

Introduction

Hippocampal coding multiplexes over broad temporal scales incorporating prior, current, and future contextual information [1,2]. Among pyramidal cells of hippocampal CA1, transient firing rate increases lasting from hundreds to thousands of milliseconds encode the position of an animal within a specific environment ('place cells;[3,4]), signal goal-locations [5], mark time intervals [6], respond to specific odors [7], sounds [8], objects [9] and, in humans, to other people's identities [10]. The information required to form these multimodal representations [11], converges to the hippocampus from cortical and subcortical regions [12], building context-specific cognitive rate-maps [13,14].

In conjunction with rate coding, hippocampal units also coordinate at much faster temporal scales, entrained to the dominant state-dependent oscillations of the local field potential (LFP): 5-10 Hz theta rhythms, during active exploration and REM sleep, and sharpwave-ripples during immobility and non-REM sleep. Theta phase precession [15], theta sequences [16], and ripple-associated replay [17] produce single- or multi-unit activity patterns with temporal precision on the order of tens of milliseconds. During phase precession, the spiking phase of a place cell with respect to the ongoing theta oscillation shifts to earlier times in the cycle as the animal moves through that unit's spatial receptive field ('place field'). At the population level, the temporally ordered, sequential activation of place cells within a theta cycle gives rise to characteristic theta sequences. Both processes provide a temporal code for spatial information: during phase precession the position of the animal within a cell's place field correlates with theta phase of that cell's spikes [15], while theta sequences reflect past and imminent trajectories [18,19]. Moreover, in addition to spatial information, recent studies on goal-directed behaviors have uncovered theta sequences reflecting current goals [20,21] and hypothetical future experiences [22], suggesting contributions of hippocampal temporal coding to planning and speculation.

Despite their different time scales, the processes governing hippocampal rate and temporal coding are not independent. Firstly, the order in which units activate during theta cycles and replays reflects in large part the sequences in which place fields are crossed by the animal during exploration (but see also [23]). Secondly, the interplay between fast somatic inhibition and slow dendritic depolarization as the animal crosses the respective neuron's place field has been proposed as a possible mechanism behind phase precession [24–27]. Despite evidence for cross-temporal dependencies, the functional implications of these interactions for hippocampal information processing remain equivocal.

Here, we ask whether the conjunction of firing rate and phase (temporal) coding regimens endows place cell networks with refined information processing capacities, integrating contextual rate information into phase coding and differentiating between visits to the same locations under different cognitive demands. We therefore used a recently-developed method for unsupervised detection of functional assemblies to quantify how the information encoded by rate assemblies at 100 ms - 1 s timescales can affect the < 100 ms temporal coding of their constituent units in the CA1 region of rats performing a spatial working memory task. Under these conditions, we found that both theta phase and firing rate of place cells shift when the cell activates within different assemblies recruited according to task trial demands. Rate and temporal codes therefore coalesce, allowing CA1 populations to parse repeated visits to the same locations into different episodic contexts.

Results

Five adult Long Evans rats were trained to perform a spatial working memory decision making task on an end-to-end T-maze. During each trial, rats learned to run from one side of the maze to the opposite to collect 0.1 ml of sucrose solution at reward locations. Trials were subdivided into free choice and guided runs. During choice runs, rats started from one of the two reward locations marked with 'G' in **Fig. 1a** and were directed by a moveable door to turn right (from G1) or left (from G2) into the central arm of the maze. Having traversed the central arm, rats had to choose whether to turn right or left at the open T-junction to continue towards the reward locations in 'C'. A correct choice required rats to leave the central arm by turning in the same direction as they entered it (i.e. correct runs were from G1-C1 or G2-C2). Reward was delivered only upon correct trials. Choice trials were followed by guided trials that led the rats back to the 'G' side of the maze via a pair of predetermined turns guided by motorized moveable doors. All guided runs ended with reward. Data presented here are from rats that had learned task rules over between 16-23 days of habituation and training, and were performing 40 trials per recording session at between 71-90% correct. A total of 163 units was recorded from the dorsal CA1 (**Supplementary Fig. 1**) during 10 recording sessions from 5 rats. Among these, we isolated putative place cells by selecting units with a mean firing rate between 0.2 Hz and 4 Hz and with spatial information above 0.5 bits/s [28]. The remaining 131 units were used in the following analyses.

Functional cell assemblies were identified with the unsupervised machine learning algorithm for Cell Assembly Detection (CAD) [29]. CAD detects and tests arbitrary multi-unit activity patterns that re-occur more frequently than chance in parallel single-unit recordings. The algorithm automatically corrects for non-stationarity in the units' activities and scans spike count time series at multiple temporal resolutions, returning the characteristic timescales at which individual assembly patterns coordinate. Thanks to a flexible agglomeration algorithm, CAD can detect assemblies with any activity pattern, avoiding *a priori* limits on the characteristics of the detected motifs. In this manuscript, we refer to functional cell assemblies as any group of units whose activation coordinates with temporal precision between 5 msec and 5 sec, in arbitrary but consistently reoccurring patterns.

The two timescales of hippocampal assemblies

The temporal precision of hippocampal assemblies active during the task ranged from milliseconds to seconds, with a strongly bimodal distribution. Detected assemblies fell into two major groups: (1) sharp spike patterns with a median of 10% of contributing neurons (sparsity) and a temporal precision in the range of 0.006 - 0.06 sec centered around 0.028 sec (*spike-assemblies*) and (2) broader firing rate patterns with a median of about 20% contributing units and temporal precisions between 0.07 - 3 sec (*rate-assemblies*) (**Fig. 1b**). This segregation into different timescales did not, however, correspond to different hippocampal cell populations; rather, spike- and rate-assemblies were composed of largely overlapping populations. About 81% of assembly units participated in assemblies at both time scales. Moreover, two units taking part in the same spike-assembly were more likely to join the same rate-assembly than expected by chance (average probability of 0.9 against a chance level of 0.2). This indicates that the same sets of hippocampal units coordinated at temporal precisions of both tens and hundreds of milliseconds.

In order to understand the origin of these two characteristic time scales, we examined assembly activations in space and time. **Figure 1** shows representative examples of activity patterns (**Figs. 1d, e**) and place fields (**Figs. 1f, g**) for both assembly groups. Rate-assemblies

reflected the simultaneous or sequential activation of the place fields of their constituent units activated in specific maze locations and/or along task relevant trajectories, respectively (**Supplementary Fig. 2**). Their characteristic temporal scale, ranging from hundred milliseconds to seconds, was indeed compatible with the time needed by the animal to traverse the place field of a unit. Spike-assemblies, instead, had a more localized activation (with average spatial information of 2.61±0.08 vs. 2.03±0.05 for rate-assemblies, unpaired t-test, $p = 3.5\ 10^{-10}$, df = 423) which appeared to be coordinated with the theta rhythm of the local field potential (**Fig. 1d**).

Spike-assemblies fire spikes phase-locked to the local theta rhythm

To quantify the relationships between assembly activations and the theta rhythm, we isolated the spikes fired by a unit while participating in assembly activations (*assembly-spikes*, in red in **Fig. 2a**) and compared their theta phase preference with the overall firing phase preference of that unit (in black in **Fig. 2a**). We found that both spike- and rate-assemblies were similarly phase modulated (paired-sample two-tailed t-test on the fraction of assembly-units with phase-locked assembly-spikes per animal in spike- vs rate-assemblies: p = 0.9, df = 7, **Fig. 2b**), with about 69% assembly-units phase-locked when active within an assembly configuration (all fractions presented here are computed after Benjamini–Hochberg correction for multiple comparisons, see Methods for Hodges-Ajne test on phase locking). Yet, the percentage of assemblies with a stronger phase modulation during assembly activity when compared to the overall activity of the constituent units was higher for spike-assemblies (71%) than for rate-assemblies (28%) (paired-sample two-tailed t-test on the fraction of assembly-units per animal in spike- vs rate-assemblies: $p = 4.7\ 10^{-07}$, df = 7, **Figs. 2c,d**). Thus, while theta-modulated units contribute to both spike- and rate-assemblies, rate-assembly activations did not specifically coincide with temporal windows of high theta modulation. On the other hand, the higher temporal precision of spike-assemblies was associated with enhanced phase-locking of their contributing members when active within the assembly configuration.

Individual units change phase preference when active in different assemblies

As single units were often contributors to multiple assemblies (cf. **Fig. 1c**) and assemblies activated with a characteristic phase preference (cf. **Fig. 2b**), we wondered whether the phase preference of hippocampal units is an assembly-specific property rather than a unit-specific one. In other words, do hippocampal units change their phase preference when active in different assemblies? We found that among all units taking part in at least two phase-locked assemblies about 40% (fraction computed after Benjamini–Hochberg correction for multiple comparisons) changed their phase preference when active in different assemblies of the same temporal resolution (**Figs. 3a, b,** see Methods for nonparametric test on equality of median phase). This relative *phase-shift* was found both in spike- and rate-assemblies, with a slight trend toward a larger proportion of units with significant phase-shift in spike-assemblies (paired-sample two-tails t-test: p=0.08, df=7, **Fig. 3b**).

Phase coding of hippocampal assemblies

To investigate whether such shifts in phase encoded spatial or contextual information, we focused the analysis on those units changing phase when active in different assemblies and considered their activation during task epochs corresponding to different locations and cognitive demands on the end-to-end T-maze. **Fig. 3c** and **Supplementary Fig. 3** show the activation along the maze of some typical units and the assemblies they joined. While single units fired in multiple locations, assembly activations were more selective (resulting in average

spatial information of 2.21 ± 0.04 vs. 1.28 ± 0.06 for single units), typically signaling one of the place fields of their constituent units and/or only a particular run type or direction.

This enhanced selectivity suggests that theta phase coding in hippocampal units extends beyond phase precession: while phase precession relative to the ongoing theta oscillation correlates with the distance covered by the animal within a unit's place field, here we observed a phase preference disambiguating the activation of different assemblies in disjoined locations. We therefore hypothesised that theta phase coding of hippocampal units is not limited to the animal's position within a place field, but is also associated with different locations or contexts in the environment.

Place-cell firing phase can encode distinct place fields

Different phase preferences of different assemblies could in principle be explained by the phenomenon of phase precession if assemblies systematically recruited spikes from different parts of the same place field(s), thereby incorporating spikes that had precessed to different degrees. This is not what we observed (**Figs. 3** and **Supplementary Fig. 3**) but, to completely rule out this possibility, we analyzed the phase preference of single units, this time separating their spikes according to place field location instead of by assembly membership. This approach was extended to all recorded place cells, not only those detected as participating in assemblies. In fact, we assume that all CA1 place cells do participate some assembly, but that sparse electrophysiological sampling of the CA1 population precludes detection of all potential assemblies.

Above we showed that firing rate assemblies corresponded to the coordinated activation of multiple units with overlapping (simultaneous-) or neighbouring (sequential-assemblies) place fields. We also showed that single units changed their phase preference when active in different rate-assemblies (**Fig. 3b**). We therefore would expect that separating unit spikes according to their place field location would reveal shifts in phase similar to those observed when they were separated according to the assembly structure they were participating in. Accordingly, we selected all units with multiple place fields and clustered their spikes according to their firing location (**Fig. 4a**, see Methods). In our dataset, all putative place cells had more than one place field with a median of five fields per unit. Such a high number of place fields per unit was due to the relatively large size of the maze [30] and, critically, to its compartmentalization in clearly identifiable segments. Comparing the phase preference with respect to place field location, we found that 53% of the tested units changed firing phase when active in different place fields (fraction computed after Benjamini–Hochberg correction for multiple comparisons, **Figs. 4b, 5b**).

The firing phase of place-cells can encode distinct task-related information within the same place field

Beyond encoding spatial information, the hippocampus has been shown to carry information about episodic memories [31,32], sequences [33,34] and abstract relations [35,36]. Thus, hippocampal assemblies may encode task relevant information other than purely spatial parameters. We can therefore expect the recruitment of different assemblies when the animal has to remember, e.g., a left turn rather than a right turn, or has to perform a guided turn rather than a choice turn. At the single-unit level, this should be reflected by a change of a unit's phase preference for different trial types, even within the same place field.

Separating unit spikes according to place field as in the previous analysis, we further divided the spikes according to the type of trial in which they occurred. Trials were divided into: left and

right choice runs, when the animal had to choose between left and right turn, and four different types of guided run, in which the sequence of turns was predetermined by the experimenter (**Fig. 5a**). We found that 38% of units changed their phase preference when active in different trial types, despite overlapping place-field locations (**Fig. 5b**, see also **Supplementary Fig. 4a** for same analysis with spikes fired only in epochs of high theta-power). In fact, separating a unit's spikes not just by place field but according to the task epoch they were from resulted in narrower and more coherent phase distributions of a unit's spikes (**Fig. 5c**). This observation was corroborated by training a support vector machine (SVM) classifier on the phase of spikes fired in an individual place field to distinguish between trial types. We found that for 40% of units at least two trial types within at least one of their place fields could be distinguished above chance level (see Methods for details). Moreover, we found that adding information on the spike phase to the instantaneous firing rate improved the decoding performance of the SVM (paired-sample two-tailed t-test on the accuracy of a SVM classifier trained on the instantaneous firing rate of each spike vs. a SVM trained on instantaneous firing rate and phase of each spike, $p = 9.3\ 10^{-7}$. T-test computed on the subset of place fields which could distinguish above chance trial identity in the latter, more powerful, classifier).

Figure 5c shows an example unit with phase-shift coding at the choice junction of the maze, distinguishing left and right turns in choice trials and right turns in different guided trial types. Interestingly, the degree of differentiation of the unit phase is maximal when the animal has to actively remember its previous path to inform its next turn, and is absent in the guided trials when no active choice has to be made and the path covered from trial onset is identical. When examining instances of phase-shift coding among trial types, we found that the majority of phase-shifts distinguished between left vs. right choice trials and choice vs. guided trials (**Fig. 5d**, one-way ANOVA, $F(3,33) = 5.0$, $p = .006$; Tukey post-hoc comparisons indicated with respect to the figure columns: (I column, IV column) $p = 0.048$, (II column, IV column) $p = 0.016$. See also **Supplementary Fig. 4b** for same analysis with spikes fired only in epochs of high theta-power). This further supports the link between phase-shift and information encoding. The type of trial was, in fact, the most relevant information for performing the task correctly.

Phase-shift leads to context-dependent fine temporal coordination among units. The firing phase of hippocampal CA1 principal cells can therefore encode task related information to differentiate distinct maze locations or distinct mnemonic information within the same location. Such phase coding goes beyond what would be expected by phase precession. Nevertheless, phase-shifting and phase precession could share common underlying mechanisms. We observed that the population of units with phase-shift coding in at least one of their place fields correlated with the population of units with phase precession in at least one of their place fields (chi-square test for independence: $\chi^2(1,131) = 7.8, p = 0.005$, p-value threshold for significance on the test for phase precession and phase-shift of 0.05, see Methods). Phase-shifting could occur between place fields with or without phase precession (**Figs. 6a, b, c**). When place-field-dependent phase-shift and phase precession co-occurred, the spike phases covered during the precession spanned different phase ranges in the two different fields (**Fig. 6c**).

Both experimental and theoretical studies have shown how a change in excitation received by a hippocampal unit can modify its phase of discharge [24–27,37]. This suggests a possible interpretation of the phase-shift phenomena: spatial exploration or cognitive tasks recruit specific and diverse cell (rate-)assemblies; each assembly is characterized by a set of synaptic connections that provides the assembly-units with a stereotypical level of excitation whenever

the assembly is activated upon a specific task event; this assembly-specific degree of depolarization, combined with an oscillatory somatic inhibition, would thereby generate a phase preference, or phase-range preference, typical and specific for the activity of the unit within that assembly (**Fig. 6d**). In line with this hypothesis, we found that differences in average phase preference between two sets of spikes also co-occurred with differences in the average instantaneous firing rate (see Methods for methodological details). This was true when comparing spikes from different place-field locations, within the same location but from different trial types, or spikes occurring as part of different spike- or rate-assemblies (chi-square test of independence on pairs of spike-sets with p-value > or < 0.05 when testing phase and instantaneous firing rate differences: different place fields: $\chi^2(1,2171) = 12.0\,, p = 5.4\,10^{-4}$, same location: $\chi^2(1,584) = 11.4\,, p = 7.3\,10^{-4}$, spike-assemblies: $\chi^2(1,766) = 7.5, p = 0.006$, rate-assemblies: $\chi^2(1,8269) = 86.8\,, p = 0$).

Finally, as for phase precession, the fine coordination of neuron firing with the theta oscillation will generate, at the network level, a stereotypical sequence of unit activations [16]. In the case of phase-shift coding however, the sequence of active units during a theta cycle be determined not only by the spatial proximity of their place fields, but will also be affected by the identity of the assembly recruited at the time. This implies that the lag between the activation of two units within the theta cycle, and consequently the sequence order and composition, could vary according to the cognitive demand. We investigated this hypothesis by testing if the lag of maximal cross-correlation between two units within a theta cycle changed in different trial types (**Fig. 6e**). To make sure that such a change was not due to occasional outliers but was consistent across trials, we selected the lag of maximal cross-correlation for each trial and compared the set of lags so obtained by trial type. We performed the analysis for each place field of each unit and found that changes in cross-correlation lags occurred with higher probability in place fields where units displayed phase-shift coding across trials (chi-square test of independence on $\chi^2(1,203) = 5.3\,, p = 0.02$).

To explore how the activation of different rate assemblies can produce different activation sequences along the theta cycle even within the same set of units, we simulated the phenomenon with an adaptive exponential integrate-and-fire model [38] (see Methods for formal description of the model). As observed in the experimental data, single units could participate in multiple assemblies (cf. **Fig. 3**) and respond at different, but context-consistent, average firing rates (cf. **Fig. 5**). We simulated three units taking part in two rate assemblies. During the assembly activation, each unit received an assembly-specific degree of depolarization. Assembly retrieval was modelled by the synchronous and transient depolarization of its constituent units, while inhibition was on average constant over time, and identical for all units and both assemblies. Similarly to soma-dendritic interference models [25,27,37], we captured the interplay between the oscillatory inputs to units by sinusoidally modulating both excitatory and inhibitory conductances with a relative offset of π rad (**Fig. 6f top**). As expected, assembly activations produced a broad increase in unit firing rate punctuated by faster temporal coordination with the theta oscillation (**Fig. 6f bottom**). To formally detect multi-unit activity patterns generated by the assembly activations, we simulated multiple retrievals of the two assemblies and analysed the obtained spike trains with CAD*opti* assembly detection algorithm, as previously done with our experimental dataset (see Methods and **Supplementary Table 1** for simulations details and CAD*opti* parameters). The activation of both assemblies produced, at a fine temporal scale, sequential activity patterns with a mean lag of 0.06 ± 0.005 sec and 0.07 ± 0.005 sec of the second and the third unit from the first active. Despite the similarity in pattern structure, the two assemblies triggered a different activation order of their constituent

units. In 98% of the simulations (n = 100 simulations performed with different noise realizations), the detected activation sequence reflected the assembly-specific degree of depolarization provided to each unit (**Fig. 6f inset**). More generally, units that received the highest depolarization activated first within the theta cycle while, importantly, units receiving just a light depolarization terminated the activation sequence.

Overall, these results highlight how phase-shift coding not only broadens the range of information encoded by the hippocampal temporal coding but also contributes to the generation of context-specific theta sequences.

Discussion

The present study investigated phase coding by CA1 cell assemblies in a spatial working memory task. The unsupervised detection of functional assemblies confirmed that hippocampal coding is characterized by two predominant time scales: a rate scale ('rate assemblies'), compatible with place field rate coding, and a much finer temporal scale ('spike assemblies'), in agreement with the fine coordination of spikes within the theta band of the local LFP. We found that units that participated in a given spike-assembly often co-participated in a rate-assembly as well. This is in line with the observation that cells with neighbouring place fields engage in both phase- and rate-coordination [16,39]. Both spike- and rate-assemblies activated in coordination with the theta oscillation, in line with a large body of literature on hippocampal assemblies [40–42]. In particular, it has been shown that CA1 neurons enhance their phase-locking with the ongoing theta rhythm when active within an assembly configuration [42]. Here, we showed that such enhanced locking is due to the coordination within spike-assemblies and is reflected in rate-assemblies because of the spike-assemblies nested within them.

The enhanced phase modulation of hippocampal units during assembly activations also revealed that units taking part in multiple assemblies changed their preferred spiking phase according to the assembly active at the time. This shift often coincided with a change in the place-field of activation of the unit when active in one or the other assembly. The observed higher specificity of information coding by assemblies with respect to that of the participating units therefore agreed with the higher specificity in phase preference exhibited by single units when active as part of the assembly. This was true both for spike- and rate-assemblies, and was confirmed at the single-unit level when unit spikes were grouped by place field rather than by assembly identity. Importantly, phase-shift coding was not limited to spatial information but, in addition, reflected other cognitive variables. Specifically, we found that – even when active in the same place field – units changed their phase preference in accordance with different contextual conditions and task variables. These changes were fast and reversible, in line with the hypothesis that they were generated by the transient activation of different cell assemblies. This extends the framework proposed in a recent study suggesting that the balance between rate and phase coding of spatial information by anatomically distinct place cell subpopulations may reflect current (fixed) sensory cue conditions [43]; our results show that integration of rate and phase coding *within* a population supports dynamic coding of episodic information in response to varying cognitive load.

Despite the differences in the type of information encoded, phase-shift coding and phase precession might be generated by the same underlying mechanism. The models proposed to

explain phase precession divide broadly into three categories: phase precession through interference between the oscillation of the somatic membrane potential at theta and the oscillation of the dendritic potential at a slightly higher frequency [15,44], through a progressive dendritic depolarization coupled with somatic oscillatory inhibition [24–27], and through the pattern of synaptic transmission delays [45]. To this day, unanimous agreement on the mechanism behind phase precession is yet to be reached and it is beyond the scope of this manuscript to validate one or the other hypothesis. In order to address these various hypotheses, numerous experimental efforts have been made to elucidate the relationship between cell depolarization and spiking phase. It has been observed that while the animal moves towards the center of a cell's place field, rate and phase of spiking strongly correlate [25,27]. This correlation is, however, lost as the rate peak is passed and the animal leaves the cell's place field [46]. In vivo whole-cell recordings have shown that during phase precession the baseline membrane potential of CA1 pyramidal neurons undergoes a ramp-like depolarization [47]. In vitro, whole-cell patch-clamp recordings from dendrites and somata showed that an increase in dendritic excitation, coupled with phasic somatic inhibition, causes an increase in the neuron's firing and the advancement of the spiking phase with respect to the somatic modulation [26,37]. Similar results were observed when progressively depolarizing the membrane potential of hippocampal cells in anesthetized animals [24]. Thus, despite the asymmetry in rate-phase coupling before and after the rate peak is reached, possibly caused by activity-dependent changes in the perisomatic inhibition [37], this evidence shows how changes in depolarization lead to changes in discharge phase. In line with these observations we found that the changes in phase preference also co-occurred with changes in the instantaneous firing rate of the unit. We therefore propose that phase-shift coding may be a consequence of the different levels of depolarization provided by the specific synaptic embedding within different assemblies activated as the animal encounters different cognitive challenges or environmental factors (cf. **Fig. 6d**).

The fine temporal coordination of unit activities imposed by phase precession aligns with plasticity mechanisms for imprinting episodic information that, otherwise, would be separated by seconds. For this reason, phase precession has been proposed as a network mechanism for episodic sequence learning [1,16,27,48–51]. In support of this hypothesis, studies showed that degradation of the temporal coordination of hippocampal units with the theta rhythm, e.g. by the administration of the cannabinoid receptor agonist [52] or by muscimol injection into the medial septum [53], led to reduced performance in memory tasks despite maintaining an intact place-field representation. Moreover, degraded phase precession caused by the passive transportation of rats during spatial exploration, drastically reduced replay during subsequent sleep [54], a signature of impaired memory consolidation [55–57]. The changes in assembly-specific phase preference of hippocampal units reported here allow for recombination in the activation sequences along the theta cycle. This could contribute to the formation of context-dependent theta sequences, supporting the formation of episodic memories and planning [22].

Goal-dependent theta sequences have been observed during decision-making tasks, where the theta sequences terminated with the activation of cells encoding distant goal-locations [20]. In a recent study, theta sequences encoding alternative future decisions have been shown to alternate in consecutive theta cycles as the animal approached the choice location [22]. The process by which goal-related theta sequences form is still unclear, as is the causal relation between phase precession and theta sequences (see [58] for review). A possible hypothesis is that during the early stages of learning, inter-regional assemblies (e.g. prefrontal-hippocampal assemblies [59–61] or medial-septum-hippocampal assemblies [62]), recruited at each theta cycle [63], modulate the depolarization of hippocampal units thereby dynamically producing

goal-dependent cycling activity. In particular, as implied by our theoretical model (cf. **Fig. 6f**), a low-level generalized depolarization of cells encoding the current goal location could explain their spiking at the end of theta sequences also when the animal is far from the goal location [20]. Such assembly-specific cycling activity could then be reinforced in theta sequences through plasticity mechanisms, especially within networks rich in recurrent collaterals such as CA3. Indeed, similar mechanisms as observed here for assembly-dependent phase preference of CA1 units may also play a role in organizing phase preferences of neurons across other brain regions, consistent with evidence for phase precession in the dentate gyrus [64], CA3 [64,65], entorhinal cortex [64,66], subiculum [67], ventral striatum [68] and in the medial prefrontal cortex [69]. Such distributed processing would therefore support the integration of spatial and temporal information into cognitive contexts at a timescale commensurate with rapid adaptive behaviors, dynamically aligning different hippocampal assemblies with different subsets of neocortical and subcortical neurons.

Acknowledgments

We would like to thank Richard J. Gardner for spike sorting, Andreas Draguhn and Martin Both for their support and the stimulating discussions, and Thomas McHugh and David Foster for commenting on the manuscript. The drawing of the rat in Figure 6 has been modified from https://scidraw.io/. The work was supported by the Ch. and H. Schaller Foundation and by the Boehringer Ingelheim Foundation grant 'Complex Systems' to ER, and by funds to DD from the Deutsche Forschungsgemeinschaft (DFG) within CRC-1134 (subproject D01) and through individual grant Du 354/10-1. Data acquisition was supported by BBSRC grant BB/G006687/1 awarded to MWJ and a Newton International Fellowship awarded to NB, with further analyses supported by a Wellcome Senior Research Fellowship to MWJ (202810/Z/16/Z).

Author contributions

Experimental design and Electrophysiology, NB and MWJ; Analysis, Visualization and Interpretation, ER; Writing - Original Draft, ER; Writing - Review and Editing, MWJ, APFD and DD; Resources, MWJ, and DD; Funding Acquisition, ER, NB, MWJ, and DD.

Competing Interests

The authors declare no competing interests.

Data availability

All data reported in this study are available from the corresponding authors upon request.

Code availability

Code for cell assembly detection at multiple time scales CAD and CAD*opti* available at https://github.com/DurstewitzLab/Cell-Assembly-Detection and https://github.com/DurstewitzLab/CADopti, respectively.

Figures

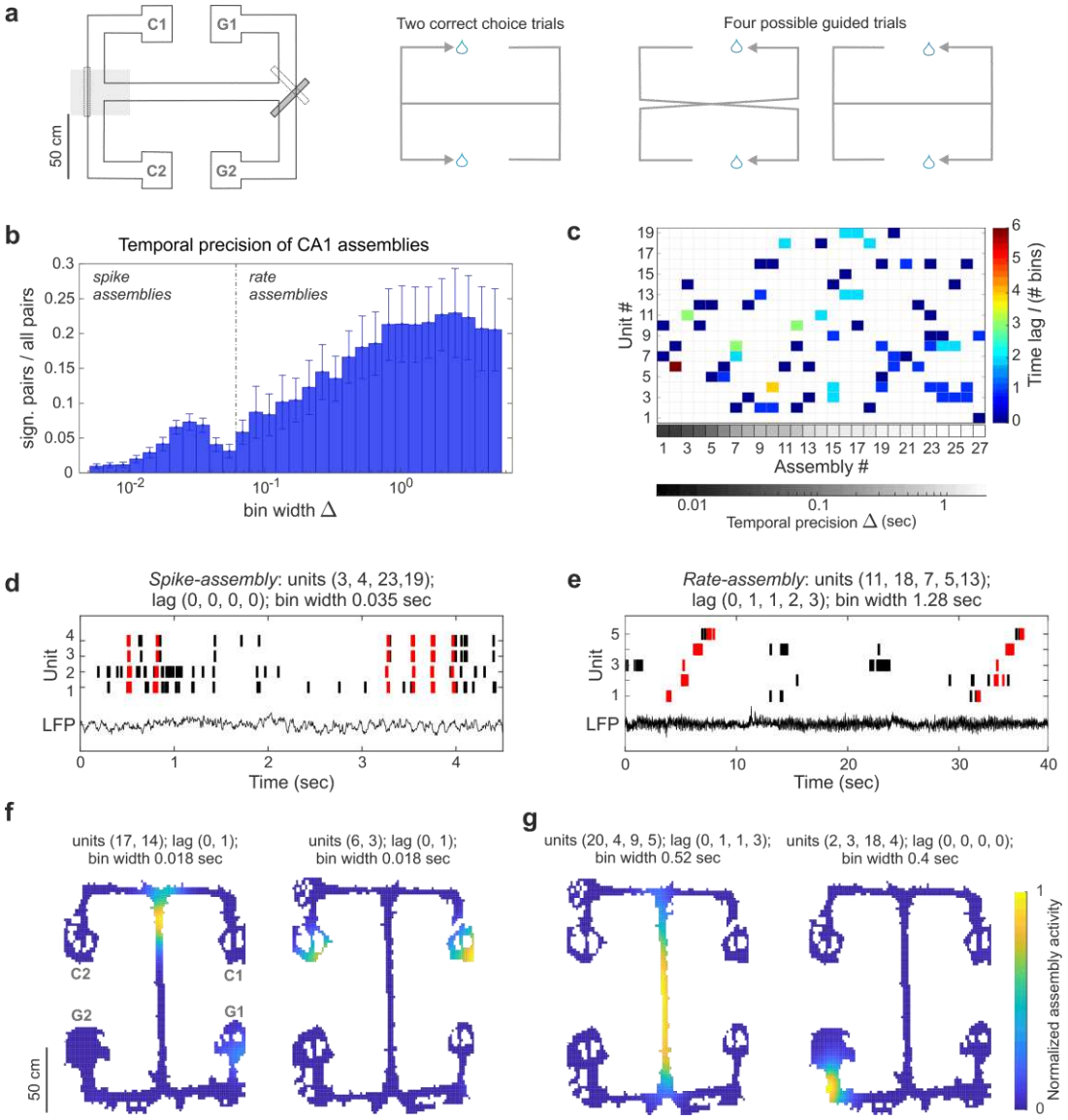

Figure 1 | The two timescales of hippocampal assemblies. (a) Maze and task schematic. Task trials constitute choice and guided runs. In choice runs, the animal runs in direction G→C, deciding between left or right turns at the T-junction marked in gray. Correct choice is contingent upon starting location. In guided trials the animal run in direction C→G, following a predetermined path guided by motorized moveable doors; (b)The distribution of the temporal precision of the assemblies detected during the spatial working memory task shows the presence of two predominant time scales: one peaked around 28 ms and one on the second scale. Bars show mean and SE computed across animals. CAD parameters: ref_lag=2, no pruning; (c) Assembly-assignment matrix for one exemplary data set. The grayscale indicates the temporal resolution at which assemblies are detected; the color scale shows the lag between the activation of each assembly-unit with respect to the unit first active in the assembly. Hippocampal place cell units were typically found part of multiple assemblies; (d, e) Examples of spike- (d) and rate- (e) assembly activity patterns (red) and raw LFP. Tempor al resolution, composing units and lag of activation of each unit with respect to the activation of the first assembly-unit are indicated in the figure. Spike-assembly activations appear to be locked to the theta rhythm of the LFP; (f, g) Example of spike- (f) and rate- (g) assembly place fields. See also **Supplementary Fig. 2** for place fields of the relative assembly composing units.

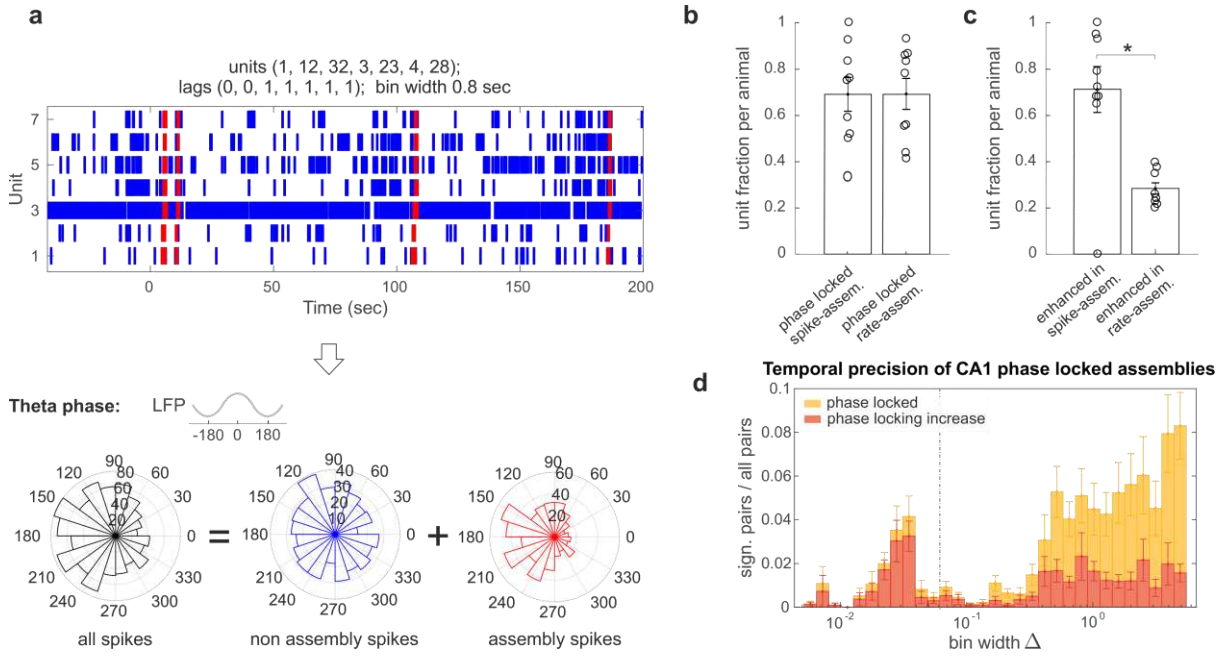

Figure 2 | Spike-assemblies fire phase locked spikes. (a) Raster plot of one typical assembly and its composing units (spikes fired during assembly activations marked in red). Below, phase histogram of the spikes of one exemplary unit showing how assembly spikes (red) have an enhanced phase modulation with respect to either all (black) or non-assembly (blue) spikes; (b) Fraction of units with phase-modulated assembly-spikes and (c) units with assembly-spikes with enhanced phase-modulation with respect to the totality of the unit spikes (i.e. red vs. black in (a)) in at least one of the assemblies they take part in. Mean and SE computed across animals after Benjamini–Hochberg correction for multiple comparisons, data points correspond to the 10 individual recording sessions; (d) Temporal precision of spike- and rate- assemblies with phase-modulated spikes (yellow) and assemblies with spikes with enhanced phase-modulation with respect to their composing units (red). Displayed assemblies separately pruned in the two time scales (see Methods). Bars show mean and SE pooled from all sessions. While the activity of both spike- and rate-assemblies is theta modulated, only spike-assemblies coordinate with the LFP more than their composing units.

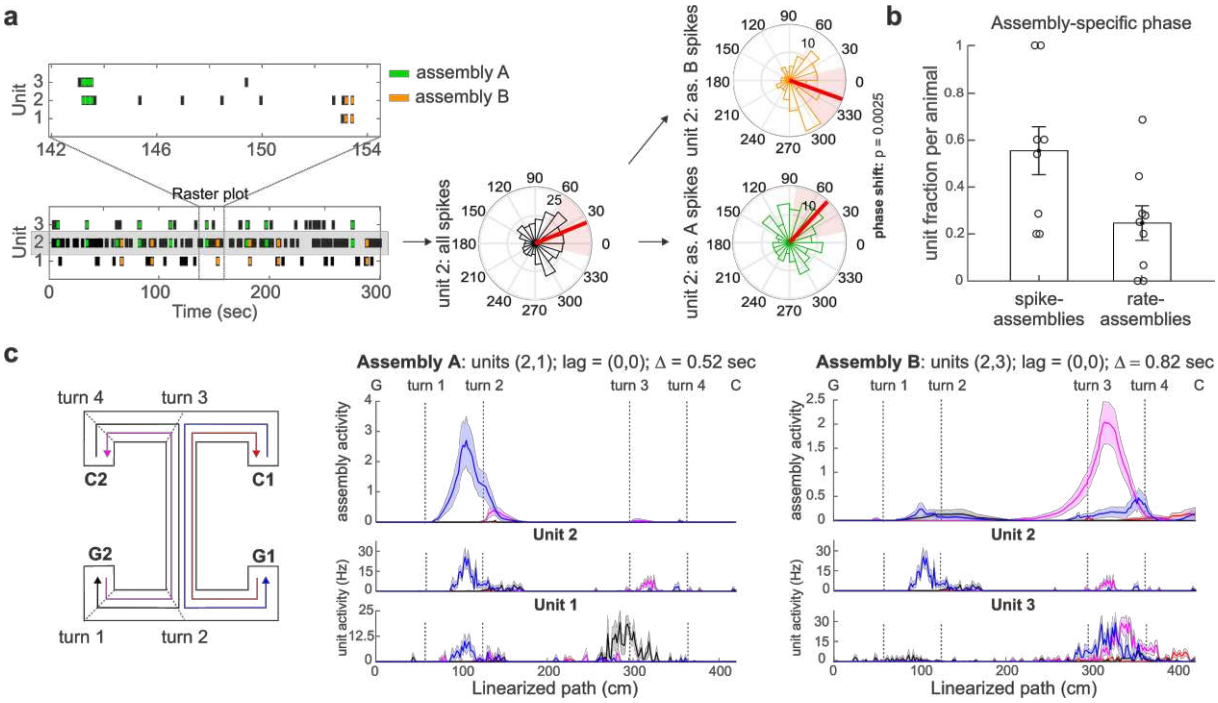

Figure 3 | Single units change phase preference when active in different assemblies. (a) Raster plot and phase preference of two assemblies with a shared unit (unit 2). Unit 2 changes phase preference when active in the two different assembly configurations; (b) Fraction of units that change their phase preference when active in different assemblies. Mean and SE computed across animals after Benjamini–Hochberg multiple comparison correction, data points correspond to distinct recording sessions; (c) Activation along the maze for different trial types of the two assemblies in (a) and their composing units. The trial typologies displayed are: left (pink) and right (red) choice trials, and left (blue) and right (black) guided trials. The assembly and unit activity are plotted along the linearized path. Vertical dashed lines mark different task segments, along the path from C to G, as indicated in the maze scheme for the left choice trial. Assembly temporal resolution, composing units and lag of activation of each unit with respect to the activation of the first assembly-unit are indicated in the figure. The change in firing phase of unit 2 when active within assembly A and B (a) is associated with a change in encoded information of the two assemblies (c). See also **Supplementary Fig. 3** for other examples of assembly-dependent phase modulation of CA1 units.

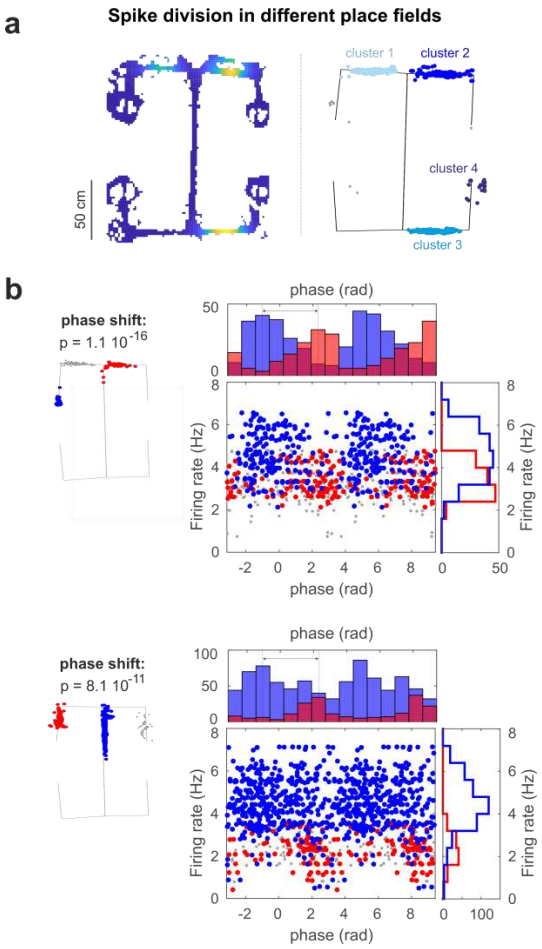

Figure 4 | Place-cells firing phase can encode distinct place fields. (a) Example of unsupervised spike clustering based on the spike position in a unit with multiple place fields. The number of place fields present in the spike set was established with DBSCAN, a density-based spatial clustering algorithm. The cluster memberships resulting from DBBSCAN were then fed to a Gaussian mixture model for the final step of the classification. (b) Rate-phase and respective marginal distributions of a unit spikes color-coded according to their field of firing. The exemplary units changed their firing phase when active in different place fields.

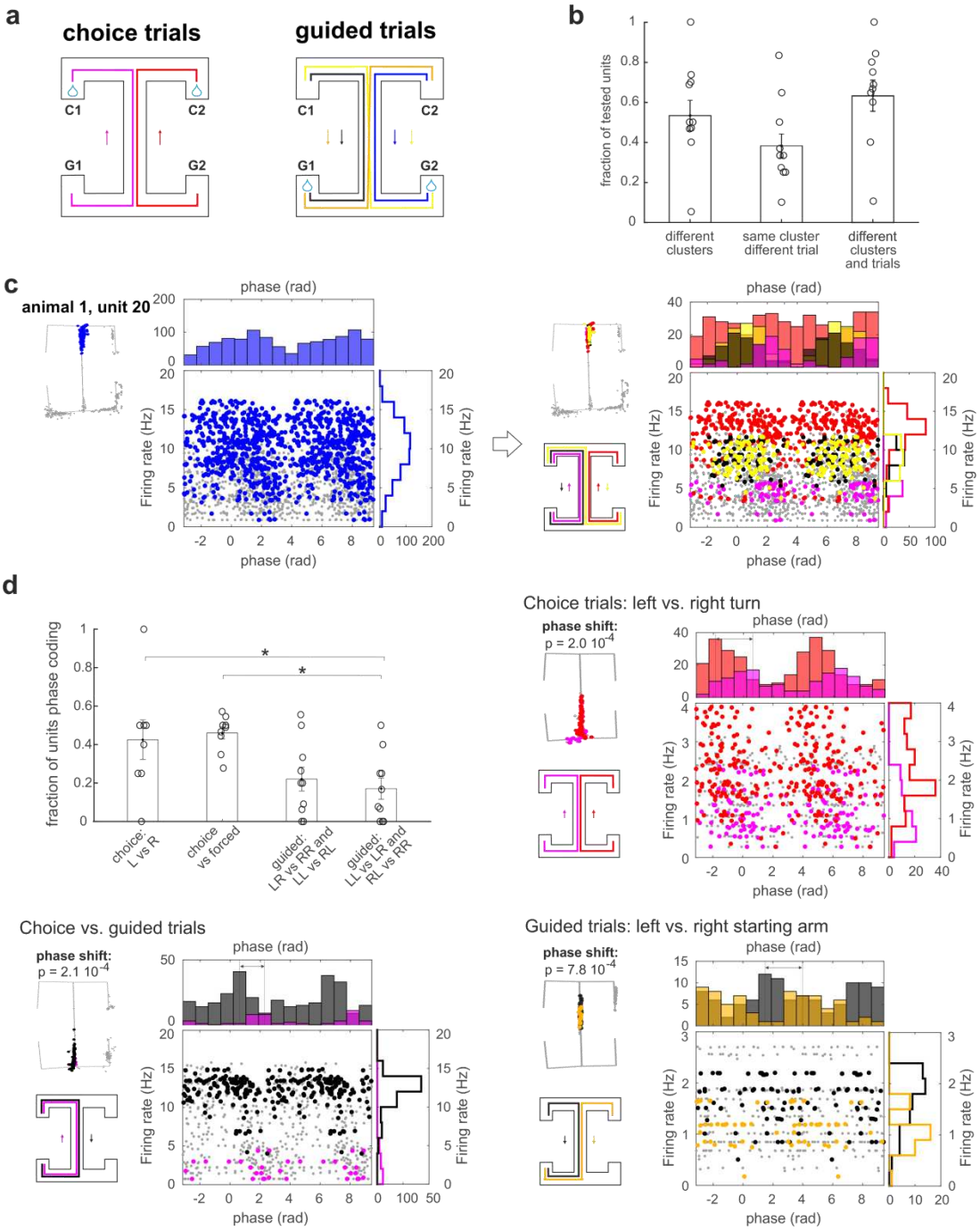

Figure 5 | The firing phase of place-cells can encode distinct task-related information within the same place field. (a) Trial categories: choice left (magenta), choice right (red), forced left (LL, blue), forced right (RR, black), forced switch right-left (RL, light yellow) forced switch left-right (LR, dark yellow); (b) fraction of units changing phase for different locations irrespective of the trial type, different trial types but same location; different trial type and/or location; (c) joint rate-phase distribution and marginal distributions for the spikes fired by a unit in one of its place fields (left panel, blue) and the same spikes divided by trial type (right panel, colour coding of to trial type specified in (a)); (d) fraction of units changing phase when comparing: left vs. right choice trials; choice vs. forced trials; forced trials with different origin arms; forced trials with same origin arms but different forced turn. Mean and SE in (b) and (c) are computed across animals after Benjamini–Hochberg correction for multiple comparisons, data points correspond to distinct recording sessions.

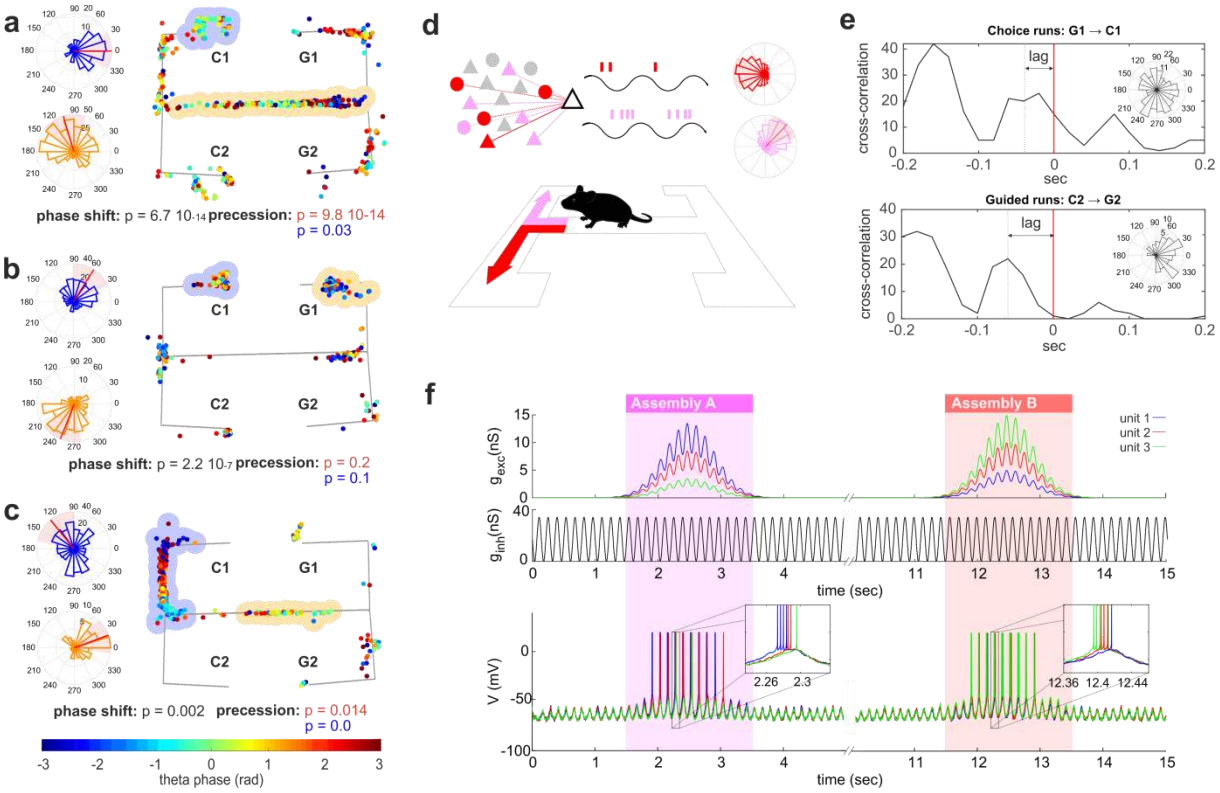

Figure 6 | Phase-shift leads to context-dependent fine temporal coordination among units. (a) Spike phase (color-coded) and location of three units with multiple place fields. On the left, phase histogram of all spikes fired in the place fields marked in blue and yellow. All three units show a change in phase preference when active in different locations. Phase-shift could occur between place field with (a-c) and without (b) phase precession. See Methods for tests on phase-shift and phase precession, p-values indicated in the figure; (d) Schematic of assembly-specific phase coding: In order to perform a task, or a choice, we are required to recall past information and future goals. Different contextual conditions will therefore trigger the retrieval of different assemblies even within a same location. By providing different degrees of depolarization, the retrieval of each assembly will set for their member-units assembly-specific ranges of firing phase; (e) Cross-correlation between the spikes of two units during choice (above) and guided (below) right trials. Phase histogram of A spikes are shown as inset for the two trial types. Unit A changes firing phase when active in choice and guided trials (p = 0.03), thereby changing its relative lag of activation with unit B during theta cycles (two-tailed Wilcoxon rank sum test, p = 0.01). Phase-shift coding can therefore produce context-dependent theta sequences. (f) Simulation of the recruitment of three neurons by two rate assemblies. (top) Excitatory and inhibitory conductances of three neurons (blue, red and green) modelled with an adaptive exponential integrate-and-fire model. The activation of rate assembly A and B was modelled with a transient unit-specific increase in excitatory conductances g_{exc} and a shared oscillatory inhibition g_{inh}. (bottom) Membrane potential V of the simulated units during assembly retrieval. The order in unit activation along the theta cycle reflects the intensity of the assembly-specific depolarization provided to the units (inset).

References

1. Colgin, L. L. Rhythms of the hippocampal network. *Nat. Rev. Neurosci.* **17**, 239–249 (2016).

2. Buzsáki, G. & Watson, B. O. Brain rhythms and neural syntax: Implications for efficient coding of cognitive content and neuropsychiatric disease. *Dialogues Clin. Neurosci.* **14**, 345–367 (2012).

3. Muller, R. U. & Kubie, J. L. The effects of changes in the environment on the spatial firing of hippocampal complex-spike cells. *J. Neurosci.* **7**, 1951–1968 (1987).

4. O'Keefe, J. & Dostrovsky, J. The hippocampus as a spatial map. Preliminary evidence from unit activity in the freely-moving rat. *Brain Res.* **34**, 171–175 (1971).

5. Hok, V. *et al.* Goal-related activity in hippocampal place cells. *J. Neurosci.* **27**, 472–482 (2007).

6. Eichenbaum, H. Time cells in the hippocampus: A new dimension for mapping memories. *Nature Reviews Neuroscience* **15**, 732–744 (2014).

7. Eichenbaum, H., Kuperstein, M., Fagan, A. & Nagode, J. Cue-sampling and goal-approach correlates of hippocampal unit activity in rats performing an odor-discrimination task. *J. Neurosci.* **7**, 716–732 (1987).

8. Aronov, D., Nevers, R. & Tank, D. W. Mapping of a non-spatial dimension by the hippocampal-entorhinal circuit. *Nature* **543**, 719–722 (2017).

9. Fried, I., MacDonald, K. A. & Wilson, C. L. Single neuron activity in human hippocampus and amygdala during recognition of faces and objects. *Neuron* **18**, 753–765 (1997).

10. Rey, H. G. *et al.* Single Neuron Coding of Identity in the Human Hippocampal Formation. *Curr. Biol.* **30**, 1152-1159.e3 (2020).

11. Quian Quiroga, R., Kraskov, A., Koch, C. & Fried, I. Explicit Encoding of Multimodal Percepts by Single Neurons in the Human Brain. *Curr. Biol.* **19**, 1308–1313 (2009).

12. Van Strien, N. M., Cappaert, N. L. M. & Witter, M. P. The anatomy of memory: An interactive overview of the parahippocampal- hippocampal network. *Nature Reviews Neuroscience* **10**, 272–282 (2009).

13. Lisman, J. *et al.* How the hippocampus contributes to memory, navigation and cognition. *Nat. Neurosci.* **20**, 1 (2017).

14. O'Keefe, J. & Nadel, L. *The Hippocampus as a Cognitive Map*. (Oxford University Press, 1978).

15. O'Keefe, J. & Recce, M. L. Phase relationship between hippocampal place units and the EEG theta rhythm. *Hippocampus* **3**, 317–330 (1993).

16. Skaggs, W. E., McNaughton, B. L., Wilson, M. A. & Barnes, C. A. Theta phase precession in hippocampal neuronal populations and the compression of temporal sequences. *Hippocampus* **6**, 149–172 (1996).

17. Lee, A. K. & Wilson, M. A. Memory of Sequential Experience in the Hippocampus during Slow Wave Sleep. *Neuron* **36**, 1183–1194 (2002).

18. Huxter, J. R., Senior, T. J., Allen, K. & Csicsvari, J. Theta phase-specific codes for two-dimensional position, trajectory and heading in the hippocampus. *Nat. Neurosci.* **11**, 587–594 (2008).

19. Gupta, A. S., Van Der Meer, M. A. A., Touretzky, D. S. & Redish, A. D. Segmentation of spatial experience by hippocampal theta sequences. *Nat. Neurosci.* **15**, 1032–1039 (2012).

20. Wikenheiser, A. M. & Redish, A. D. Hippocampal theta sequences reflect current goals. *Nat. Neurosci.* **18**, 289–294 (2015).

21. Johnson, A. & Redish, A. D. Neural ensembles in CA3 transiently encode paths forward of the animal at a decision point. *J. Neurosci.* **27**, 12176–12189 (2007).

22. Kay, K. *et al.* Constant Sub-second Cycling between Representations of Possible Futures in the Hippocampus. *Cell* **180**, 552-567.e25 (2020).

23. Stella, F., Baracskay, P., O'Neill, J. & Csicsvari, J. Hippocampal Reactivation of Random Trajectories Resembling Brownian Diffusion. *Neuron* **102**, 450-461.e7 (2019).

24. Kamondi, A., Acsady, L., Wang, X.-J. & Buzáki, G. Theta oscillations in somata and dendrites of hippocampal pyramidal cells in vivo: activity-dependent phase-precession of action potentials. *Hippocampus* **8**, 244–261 (1998).

25. Harris, K. D. *et al.* Spike train dynamics predicts theta- related phase precession in hippocampal pyramidal cells. *Nature* **417**, 2116–2118 (2002).

26. Magee, J. C. Dendritic mechanisms of phase precession in hippocampal CA1 pyramidal neurons. *J. Neurophysiol.* **86**, 528–532 (2001).

27. Mehta, M. R., Lee, A. K. & Wilson, M. a. Role of experience and oscillations in transforming a rate code into a temporal code. *Nature* **417**, 741–746 (2002).

28. Skaggs, W. E., McNaughton, B. L., Gothard, K. M. & Markus, E. J. An Information-Theoretic Approach to Deciphering the Hippocampal Code. *Adv. Neural Inf. Process. Syst.* **5**, 1030–1037 (1993).

29. Russo, E. & Durstewitz, D. Cell assemblies at multiple time scales with arbitrary lag distributions. *Elife* **6:e19428**, 1–39 (2017).

30. Park, E. H., Dvorak, D. & Fenton, A. A. Ensemble place codes in hippocampus: CA1, CA3, and dentate gyrus place cells have multiple place fields in large environments. *PLoS One* **6**, 1–9 (2011).

31. Burgess, N., Maguire, E. A. & O'Keefe, J. The human hippocampus and spatial and episodic memory. *Neuron* **35**, 625–641 (2002).

32. Leutgeb, S. *et al.* Neuroscience: Independent codes for spatial and episodic memory in hippocampal neuronal ensembles. *Science (80-.).* **309**, 619–623 (2005).

33. Albouy, G. *et al.* Both the Hippocampus and Striatum Are Involved in Consolidation of Motor Sequence Memory. *Neuron* **58**, 261–272 (2008).

34. Fortin, N. J., Agster, K. L. & Eichenbaum, H. B. Critical role of the hippocampus in memory for sequences of events. *Nat. Neurosci.* **5**, 458–462 (2002).

35. Behrens, T. E. J. *et al.* What Is a Cognitive Map? Organizing Knowledge for Flexible Behavior. *Neuron* **100**, 490–509 (2018).

36. Garvert, M. M. M., Dolan, R. J. & Behrens, T. E. J. A map of abstract relational knowledge in human entorhinal cortex. *Elife* 1–20 (2017). doi:10.7554/eLife.17086

37. Losonczy, A., Zemelman, B. V., Vaziri, A. & Magee, J. C. Network mechanisms of theta related neuronal activity in hippocampal CA1 pyramidal neurons. *Nat. Neurosci.* **13**, 967–972 (2010).

38. Brette, R. & Gerstner, W. Adaptive exponential integrate-and-fire model as an effective description of neuronal activity. *J. Neurophysiol.* **94**, 3637–42 (2005).

39. Dragoi, G. & Buzsáki, G. Temporal Encoding of Place Sequences by Hippocampal Cell Assemblies. *Neuron* **50**, 145–157 (2006).

40. Harris, K. D., Csicsvari, J., Hirase, H., Dragoi, G. & Buzsáki, G. Organization of cell assemblies in the hippocampus. *Nature* **424**, 552–556 (2003).

41. Buzsáki, G. & Moser, E. I. Memory, navigation and theta rhythm in the hippocampal-entorhinal

system. *Nat. Neurosci.* **16**, 130–138 (2013).

42. Lopes-dos-Santos, V., Ribeiro, S. & Tort, A. B. L. Detecting cell assemblies in large neuronal populations. *J. Neurosci. Methods* **220**, 149–66 (2013).

43. Sharif, F., Tayebi, B., Buzsáki, G., Royer, S. & Fernandez-Ruiz, A. Subcircuits of deep and superficial CA1 place cells support efficient spatial coding across heterogeneous environments. 1–14 (2020). doi:10.1101/2020.04.17.047399

44. Lengyel, M., Szatmáry, Z. & Érdi, P. Dynamically detuned oscillations account for the coupled rate and temporal code of place cell firing. *Hippocampus* **13**, 700–714 (2003).

45. Tsodyks, M. V., Skaggs, W. E., Sejnowski, T. J. & McNaughton, B. L. Population dynamics and theta rhythm phase precession of hippocampal place cell firing: A spiking neuron model. *Hippocampus* **6**, 271–280 (1996).

46. Huxter, J., Burgess, N. & O'Keefe, J. Independent rate and temporal coding in hippocampal pyramidal cells. *Nature* **425**, 828–832 (2003).

47. Harvey, C. D., Collman, F., Dombeck, D. A. & Tank, D. W. Intracellular dynamics of hippocampal place cells during virtual navigation. *Nature* **461**, 941–946 (2009).

48. Skaggs, W. E. & McNaughton, B. L. Replay of neuronal firing sequences in rat hippocampus during sleep following spatial experience. *Science* **271**, 1870–1873 (1996).

49. Diba, K. & Buzsáki, G. Forward and reverse hippocampal place-cell sequences during ripples. *Nat. Neurosci.* **10**, 1241–1242 (2007).

50. Jaramillo, J. & Kempter, R. Phase precession: a neural code underlying episodic memory? *Curr. Opin. Neurobiol.* **43**, 130–138 (2017).

51. Yamaguchi, Y. A theory of hippocampal memory based on theta phase precession. *Biol. Cybern.* **89**, 1–9 (2003).

52. Robbe, D. & Buzsáki, G. Alteration of theta timescale dynamics of hippocampal place cells by a cannabinoid is associated with memory impairment. *J. Neurosci.* **29**, 12597–12605 (2009).

53. Wang, Y., Romani, S., Lustig, B., Leonardo, A. & Pastalkova, E. Theta sequences are essential for internally generated hippocampal firing fields. *Nat. Neurosci.* **18**, 282–288 (2015).

54. Drieu, C., Todorova, R. & Zugaro, M. Nested sequences of hippocampal assemblies during behavior support subsequent sleep replay. *Science (80-.).* **362**, 675–679 (2018).

55. Girardeau, G., Benchenane, K., Wiener, S. I., Buzsáki, G. & Zugaro, M. B. Selective suppression of hippocampal ripples impairs spatial memory. *Nat. Neurosci.* **12**, 1222–1223 (2009).

56. Ego-Stengel, V. & Wilson, M. A. Disruption of ripple-associated hippocampal activity during rest impairs spatial learning in the rat. *Hippocampus* **20**, 1–10 (2010).

57. Joo, H. R. & Frank, L. M. The hippocampal sharp wave–ripple in memory retrieval for immediate use and consolidation. *Nat. Rev. Neurosci.* **19**, 744–757 (2018).

58. Drieu, C. & Zugaro, M. Hippocampal sequences during exploration: Mechanisms and functions. *Front. Cell. Neurosci.* **13**, 1–22 (2019).

59. Schmidt, B., Duin, A. A. & Redish, A. D. Disrupting the medial prefrontal cortex alters hippocampal sequences during deliberative decision making. *J. Neurophysiol.* **121**, 1981–2000 (2019).

60. Benchenane, K. *et al.* Coherent Theta Oscillations and Reorganization of Spike Timing in the Hippocampal- Prefrontal Network upon Learning. *Neuron* **66**, 921–936 (2010).

61. Eichenbaum, H. Prefrontal-hippocampal interactions in episodic memory. *Nat. Rev. Neurosci.*

18, 547–558 (2017).

62. Aoki, Y., Igata, H., Ikegaya, Y. & Sasaki, T. The Integration of Goal-Directed Signals onto Spatial Maps of Hippocampal Place Cells. *Cell Rep.* **27**, 1516-1527.e5 (2019).

63. Jezek, K., Henriksen, E. J., Treves, A., Moser, E. I. & Moser, M. B. Theta-paced flickering between place-cell maps in the hippocampus. *Nature* **478**, 246–249 (2011).

64. Mizuseki, K., Sirota, A., Pastalkova, E. & Buzsáki, G. Theta Oscillations Provide Temporal Windows for Local Circuit Computation in the Entorhinal-Hippocampal Loop. *Neuron* **64**, 267–280 (2009).

65. Mizuseki, K., Royer, S., Diba, K. & Buzsáki, G. Activity dynamics and behavioral correlates of CA3 and CA1 hippocampal pyramidal neurons. *Hippocampus* **22**, 1659–1680 (2012).

66. Hafting, T., Fyhn, M., Bonnevie, T., Moser, M. B. & Moser, E. I. Hippocampus-independent phase precession in entorhinal grid cells. *Nature* **453**, 1248–1252 (2008).

67. Kim, S. M., Ganguli, S. & Frank, L. M. Spatial information outflow from the hippocampal circuit: Distributed spatial coding and phase precession in the subiculum. *J. Neurosci.* **32**, 11539–11558 (2012).

68. van der Meer, M. A. A. & Redish, A. D. Theta Phase Precession in Rat Ventral Striatum Links Place and Reward Information. *J. Neurosci.* **31**, 2843–2854 (2011).

69. Jones, M. W. & Wilson, M. A. Phase precession of medial prefrontal cortical activity relative to the hippocampal theta rhythm. *Hippocampus* **15**, 867–873 (2005).

Methods

Animals and husbandry. All procedures were conducted in accordance with the UK Animals (Scientific Procedures) Act 1986 and approved by the University of Bristol Animal Welfare and Ethical Review Board. Five adult male Long Evans rats (300–500g, Harlan, UK) were used in this study. Prior to surgery, rats were group-housed on a 12/12 hour light/dark cycle (lights on from 07:00–19:00) with free access to food and water. At least 1 week was allowed for animals to habituate to the new holding facility before surgery was performed. Post-surgery, animals were singly housing with additional bedding and cardboard tubes in high-roofed cages that allowed unconstrained head movement with cranial implants.

Implantation of recording array. Custom-built adjustable tetrode (twisted 12.7μm nichrome wire, Kanthal, gold-plated to 250-300kW at 1kHz) microdrives were implanted under isoflurane anaesthesia using aseptic technique and perioperative opiate analgesia. Craniotomies of diameter 1-1.5 mm were made over dorsal CA1 (AP -4.2mm, ML 3.0mm from Bregma). Implants were fixed to the skull using stainless steel screws (M1.4 × 2 mm, Newstar Fastenings) and Gentamicin bone cement (DePuy). Tetrode positions were adjusted over the course of 2–3 weeks after surgery.

Tetrode signals were amplified by headstages (HS-36, Neuralynx, MT, USA) and relayed via fine-wire tethers to a Digital Lynx system (Neuralynx), which sampled thresholded extracellular action potentials at 32 kHz (filtered at 600-6000Hz) and continuous local field potentials (LFP) at 2kHz (filtered at 0.1-475Hz) using the Cheetah software package (Neuralynx) running on a desktop PC.

Training. Once post-surgery body weight had stabilized, rats were placed on a regulated feeding regimen to maintain body weight at 85-90% of free-feeding levels. The rats were trained to perform a spatial memory-based decision-making task on an end-to-end T-maze, as described in Jones and Wilson [70] and illustrated in **Figure 1a**. Training occurred during the light phase at a similar time each day. *Habituation*: Rats were placed on the maze for 20–30 minutes without any boundaries in place. Rewards were provided at every visit to a reward zone. After 2 days, rats advanced to the next stage. *Guided trials*: Rats ran a series of 'guided' trials. Each trial consisted of a run from a reward point at one side of the maze, via the long central arm to a reward point at the opposite side. At the starting end of the maze, the opposite arm was blocked off with a barrier, guiding the rat onto the central arm. At the distal end of the central arm, a barrier blocking one of the arms (pseudorandomly selected) guided the rat to the end of the unobstructed arm, where a reward (0.1 ml of 20% sucrose solution in water) was delivered. Only one running trajectory was possible in each guided trial. In one training session, a rat was allowed to perform up to 40 trials. After a minimum of 2 days of at least 20 trials, rats advanced to the next training stage. *Full Task*: Rats performed a series of guided trials, interleaved with 'choice' trials. Choice trials differed from guided trials in that there was no barrier in place at the far end of the central arm, requiring the rat to choose a turn direction. The correct turn direction was the same direction that the rat had initially turned when entering the central arm. If the rat chose correctly, a reward was delivered at the end of the arm. If the rat chose incorrectly, it was placed back at the start and allowed to undertake the trial again, until the correct choice was made. All guided trials began at the 'C' end of the maze and ended at the 'G' end, while the interleaved choice trials ran in the opposite direction. Rats were allowed to perform up to 40/40 guided/choice trials. Learning of the task rule was assessed by the percentage of correct choices made (>70% correct trials over at least 3 consecutive

days). In this manuscript, we analyzed recordings from two days (for a total of 10 independent sessions) after the performance criterion was reached.

Histology. At the end of each experiment, the rat was deeply anaesthetized with intraperitoneal sodium pentobarbital and a small electrolytic lesion made at the tip of each tetrode (positive current of 0.3 mA for 10s). After lesions had been made on each tetrode, the rat was perfused transcardially with 0.9% saline and then 4% paraformaldehyde / 0.9% saline solution. The brain was post-fixed, transferred to a cold 30% sucrose solution for cryoprotection and cut in 50µm coronal sections on a freezing microtome. Lesion locations were compared against the corresponding sections in the Rat Brain Atlas [71] in order to determine the tetrode recording sites.

Spike sorting and cell selection. Spikes were sorted semi-automatically on the basis of waveform characteristics (waveform energy and first principal component) using KlustaKwik (K.D. Harris, http://klustakwik.sourceforge.net/), followed by manual refinement of cluster boundaries with the MClust package for MATLAB (A.D. Redish, http://redishlab.neuroscience.umn.edu). After clustering, only units with mean spike peak amplitude of > 50µV, isolation distances of ≥15 [72] and <1% of interspike intervals (ISIs) below 2 ms were retained for further analysis. Our analysis focused on putative place cells. To select putative place cells we restrict to units with firing rate between 0.2 Hz and 4 Hz and with spatial information above 0.5 bit/s on the maze [73].

Cell assembly detection. Cell assemblies were identified with the unsupervised machine learning algorithm for Cell Assembly Detection (CAD) [74] (algorithm available at https://github.com/DurstewitzLab/Cell-Assembly-Detection). CAD detects recurrent activity patterns of arbitrary structure and temporal precision in multivariate time series. The algorithm is based on a recursive scheme, at each step of which it detects and tests assemblies of progressively larger size. Detection of paired assemblies was performed stopping the agglomeration at the initial pairwise step, while full-size assemblies were detected letting the algorithm agglomerate until completion.

To uncover the temporal scales most represented in the hippocampal spike trains we ran CAD on a broad spectrum of temporal resolutions sampled with a logarithmic scale in the interval [0.005 - 5.0] sec. CAD tests multiple temporal resolutions and if the same sets of units coordinate at multiple timescales the algorithm will return all of them. This analysis revealed the presence of two distinct timescales: one between 0.005 and 0.06 sec (spike-assemblies) and a second between 0.07 and 5.0 sec (rate-assemblies). To compare the extent of phase-locking and phase shift-coding within the two assembly groups we repeated the assembly detection separately for the two time windows using CAD*opti* [75] (algorithm available at https://github.com/DurstewitzLab/CADopti). After testing multiple temporal resolutions, CAD*opti* selects and returns the timescale at which each assembly has been detected with lowest p-value. Thus, each assembly was unique within each window but could be detected in both time windows. This allowed a fair comparison between the two timescales, without the distortion given by considering as independent assemblies the same set of units detected at neighbouring temporal resolutions. Finally, we want to note that the detected assemblies can not result from the detection of spike sorting mistakes. In such a case, in fact, assemblies would have been detected at the highest temporal precision (binning of 0.0058 sec), which is not the case as shown in **Figure 1b**.

For all the analysis of this manuscript the reference lag was set at 2. Tested bin sizes: [0.0058, 0.007, 0.009, 0.011, 0.014, 0.018, 0.022, 0.028, 0.035, 0.044, 0.055, 0.07, 0.09, 0.11, 0.14, 0.17, 0.21, 0.27, 0.33, 0.42, 0.52, 0.65, 0.82, 1.0, 1.3, 1.6, 2.0, 2.5, 3.2, 4.0, 5.0] and respective maximal lag: [4, 5, 5, 5, 5, 4, 4, 4, 3, 3, 3, 2, 2, 2, 2, 2, 1, 1, 1, 1, 1, 1, 1, 1, 1, 1, 1, 1, 1, 1].

Instantaneous firing rate. Instantaneous firing rates were computed by convolving unit spikes with a Gaussian kernel with kernel size of half of the unit's mean inter-spike-interval.

Phase extraction and theta power. As first step, we made sure that the spectrogram of all recorded LFPs peaked in the theta frequency band. Then, to obtain the phase of spikes we bandpass filtered the LFP between 4Hz and 10Hz (LFP_θ) and computed the angle of the Hilbert transformation of LFP_θ at the time of each spike.

Since recent studies have shown that phase coding can occur also in presence of a lower power or irregular amplitude of the theta oscillation [76,77], the analysis reported in the main figures of the manuscript are performed with maximal sample size, including all spikes without restriction on theta power. However, to make sure that the reported results were not affected by this choice, we reproduced the most important including only spikes fired in epochs of high theta power (**Figure S4**). High theta power epochs were defined as periods in which the envelope of the LFP_θ amplitude surpassed one $\sigma(LFP_\theta)$. High amplitude, saturating movement artefacts were removed from LFP by excluding periods with $LFP_\theta > 2 * \sigma(LFP_\theta)$. This was done before computing the threshold of $\sigma(LFP_\theta)$ used to define high power periods.

Phase-locking test. Phase modulation of spike sets was tested with the Hodges-Ajne test for non-uniformity [78,79] that, unlike the more common Rayleigh test, do not assume unimodality in deviation from uniformity. The test was performed on sets bigger than 50 samples, limit imposed by the approximations performed in the test. Significance was established with an alpha value of 0.05 and Benjamini-Hochberg correction for multiple comparisons on all tests performed.

Phase-locking of assembly-spikes vs. unit-spikes. We tested via bootstrap if assembly activations elicited spikes with higher phase-locking than those overall fired by the unit. For each unit, we collected the phase of the n spikes fired in correspondence of all activations of one assembly and produced 1000 replica sets composed by the phase of n spikes randomly selected among all spikes of the same unit. For each set, we computed the length R of the mean resultant vector. P-values were established by counting the fraction of replica-sets with $R_{rep.} > R_{orig.}$. Significance was established with an alpha value of 0.05 and Benjamini-Hochberg correction for multiple comparisons on all tests performed.

Change in phase preference for spikes fired in different assemblies. For each unit taking part in multiple assemblies, we divided into separate sets the spikes fired in different assembly-pairs. Sets not phase-locked to the ongoing theta oscillation or with less than 50 spikes (limitation imposed to perform the phase-locking test) were discarded. To test the null hypothesis that for a same unit each phase-set had equal median, we performed a multi-sample nonparametric test, circular analogue to the Kruskal-Wallis test [78,80]. Significance was established with an alpha value of 0.05 and Benjamini-Hochberg correction for multiple comparisons on all tests performed.

Trial categories. We divided trials into 6 categories according to the specific task required by each trial. Trials were first divided into *choice trials*, when the animal had to choose if to turn

left or right on the basis of its position at the beginning of the trial, and *guided trials*, when turns were forced by the set-up. Both categories were then further divided according to the two turns performed entering and leaving the central arm of the maze: *left-left* / *left-right* / *right-left* / *right-right*.

Isolation of place fields. Place fields were established only for units with spatial information above 0.5 (*place cells*) and with phase modulated spikes. Spikes of each unit were divided into different clusters (place fields) on the basis of their place of firing. As pre-processing step, we established the number of clusters and a first approximate cluster memberships with a density-based spatial clustering algorithm (DBSCAN, with parameters $\varepsilon = 0.05$ and $MinPts = 10$). DBSCAN was performed with the matlab routine DBSCAN Clustering Algorithm (Yarpiz, https://www.mathworks.com/matlabcentral/fileexchange/52905-dbscan-clustering-algorithm). This first estimation of cluster membership was then used as initial condition for a second and final clustering step performed with Gaussian mixture models.

Classifier. For each place field we trained a support vector machine (SVM) classifier with linear kernel (slack variables minimized with L1 norm and box constraint = 1) to divide trials according to their category. For every two types of trials, we build 3 SVM models: one based on the spike's phase, one on the spike's instantaneous firing rate, and one on both phase and instantaneous firing rate. Spike phases are a circular quantity and can not be used directly to train the SVM. Thus, phase information was passed to the classifier as $[\cos(\theta_t), \sin(\theta_t)]$, where $\theta_t$is the phase relative to the theta band of the LFP of the spike fired at time *t*. The classifier accuracy was computed with a 50-fold cross-validation, to avoid overfitting. Significance was established via bootstrap. Bootstrapped samples were created by shuffling the trial labels. Since this step removes not only the spike-label association but also any autocorrelation in the label time series (which might affect the accuracy when performing block cross-validation), for a fair comparison, we jointly shuffled the order of the spike-label elements when training the SVM classifier on the original set. The bootstrap procedure was repeated 500 times and p-values were assigned by counting the fraction of bootstrap sets with an accuracy higher or equal of the original set.

Phase precession units. We tested phase precession for each place field of each unit. Precession was assessed separately for each trial type by computing the circular-linear correlation [78,79] between the unit phase and the position of the animal along the linearized trials-specific path when the spike was fired.

Changes in lag of activation between units along theta cycles. To assess if pairs of units significantly changed their relative lag of activation during different trial types, we first computed the maximal cross-correlation lag of the two units in each trial. Cross-correlation was computed with a 0.02 sec binning and, to remain within a theta cycle, within the [-3, 3] bin window (in **Figure 6e** we chose a larger window exclusively for visualization purposes). Once obtained the maximal correlation lag for trial, we divided the trials according to their trial type and tested for a change in lag with a two-sided Wilcoxon signed rank test. Since single units had different phase preferences in different place fields, testing was performed separately for each unit place field.

AdEx model and assembly recruitment. Neuronal activity was simulated by an Adaptive Exponential Integrate-and-Fire model [81]. In AdEx models, the evolution of the neuron membrane potential V and adaptation current w is defined by the equations:

$$C\frac{dV}{dt} = -g_L(V - E_L) + g_L\Delta_T\exp\left(\frac{V - V_T}{\Delta_T}\right) - g_e(V - E_e) - g_i(V - E_i) - w + \varepsilon \quad (1)$$

$$\tau_w\frac{dw}{dt} = a(V - E_L) - w \quad (2)$$

With membrane capacitance C, leak conductance g_L, threshold slope factor Δ_T, resting potential E_L, threshold potential V_T, adaptation time constant τ_w, and subthreshold adaptation a. Noise in the evolution of the membrane potential was introduced through the parameter $\varepsilon \sim N(0, 1.6\ 10^{-19})$. Synaptic currents were modulated through the time-dependent excitatory and inhibitory conductances $g_e(t)$ and $g_i(t)$, and the excitatory and inhibitory current reversals E_e and E_i, respectively. At every time $\bar{t}$ the membrane potential reached 0 mV, an action potential was fired and $V(\bar{t})$ was set to V_s. Afterward, both the membrane potential and the adaptation current were reset to $V(\bar{t}+1) = V_r$ and $w(\bar{t}+1) = w(\bar{t}) + b$, respectively.

To reflect the presence of theta oscillations, we modulated both excitatory and inhibitory conductances at $\theta = 7$ Hz with a relative offset of π rad. The excitatory conductance was then further modulated by a gaussian-shaped depolarization to mimic transient assemblies activation

$$g_i(t) = k_i\ (\sin(2\pi\theta\ t - \pi) + 1) \quad (3)$$

$$g_e(t) = k_e(\sin(2\pi\theta\ t) + 4)\exp\left(\frac{-(t-c)^2}{2\ \sigma^2}\right). \quad (4)$$

with $c = 2.5\ sec$ and $\sigma = 0.4\ sec$ center and standard deviation of the Gaussian, respectively. The activation of an assembly provided to its composing unit n an assembly-specific degree of depolarization k_e^n. We simulated 2 assemblies composed of 3 units. In the first assembly $k_e^1 = 2.7\ nS$, $k_e^2 = 1.7\ nS$ and $k_e^1 = 0.7\ nS$. In the second assembly $k_e^1 = 1.0\ nS$, $k_e^2 = 2.0\ nS$ and $k_e^1 = 3.0\ nS$. Average inhibitory conductance was set at $k_i = 17\ nS$ for all units and all assemblies.

To formally evaluate the fine temporal coordination of network units induced by the recruitment of different context-specific cell assemblies, we concatenated 400 retrievals of each of the two modelled assemblies and ran CAD*opti* on the spike time series so obtained. We performed and analyzed 100 simulations generated with different noise realizations. CAD*opti* parameters: reference lag = 2; bin sizes: [0.0058, 0.007, 0.009, 0.011, 0.014, 0.018, 0.022, 0.028, 0.035, 0.044, 0.055]; maximal lag: [18, 21, 22, 22, 22, 20, 18, 17, 15, 13, 11].

Method references

70. Jones, M. W. & Wilson, M. A. Theta rhythms coordinate hippocampal-prefrontal interactions in a spatial memory task. *PLoS Biol.* **3**, 1–13 (2005).

71. Paxinos, G. & Watson, C. *The Rat Brain in Stereotaxic Coordinates*. (Academic Press / Elsevier, 2007).

72. Schmitzer-Torbert, N., Jackson, J., Henze, D., Harris, K. & Redish, A. D. Quantitative measures of cluster quality for use in extracellular recordings. *Neuroscience* **131**, 1–11 (2005).

73. Skaggs, W. E., McNaughton, B. L., Gothard, K. M. & Markus, E. J. An Information-Theoretic Approach to Deciphering the Hippocampal Code. *Adv. Neural Inf. Process. Syst.* **5**, 1030–1037 (1993).

74. Russo, E. & Durstewitz, D. Cell assemblies at multiple time scales with arbitrary lag distributions. *Elife* **6:e19428**, 1–39 (2017).

75. Oettl, L. L. *et al.* Phasic dopamine reinforces distinct striatal stimulus encoding in the olfactory tubercle driving dopaminergic reward prediction. *Nat. Commun.* **11**, (2020).

76. Eliav, T. *et al.* Nonoscillatory Phase Coding and Synchronization in the Bat Hippocampal Formation. *Cell* **175**, 1119-1130.e15 (2018).

77. Bush, D. & Burgess, N. Advantages and detection of phase coding in the absence of rhythmicity. *Hippocampus* 1–18 (2020). doi:10.1002/hipo.23199

78. Berens, P. CircStat: A MATLAB toolbox for circular statistics. *J. Stat. Softw.* **31**, 1–21 (2009).

79. Zar, J. H. *Biostatistical Analysis*. *Pearson* (Pearson, 2010).

80. Fisher, N. I. Statistical analysis of circular data. *Frontmatter* (1993).

81. Brette, R. & Gerstner, W. Adaptive exponential integrate-and-fire model as an effective description of neuronal activity. *J. Neurophysiol.* **94**, 3637–42 (2005).

Supplementary Information for

Integration of rate and temporal codes by hippocampal cell-assemblies supports theta phase coding of episodic information

Eleonora Russo[1,2]*, Nadine Becker[3,4], Aleks P. F. Domanski[3], Daniel Durstewitz[2,5], Matthew W. Jones[3,5]

[1] Department of Psychiatry and Psychotherapy, University Medical Center, Johannes Gutenberg University, 55131 Mainz, Germany.
[2] Dept. of Theoretical Neuroscience, Central Institute of Mental Health, Medical Faculty Mannheim, Heidelberg University, 68159 Mannheim, Germany.
[3] School of Physiology, Pharmacology & Neuroscience, Faculty of Life Sciences, University of Bristol, University Walk, Bristol BS8 1TD, UK.
[4] Current address: Nanion Technologies GmbH, Ganghoferstr. 70A, D-80339 Munich – Germany.
[5] Equal contribution.
* Corresponding author, email: eleonora.russo@zi-mannheim.de

Supplementary figures

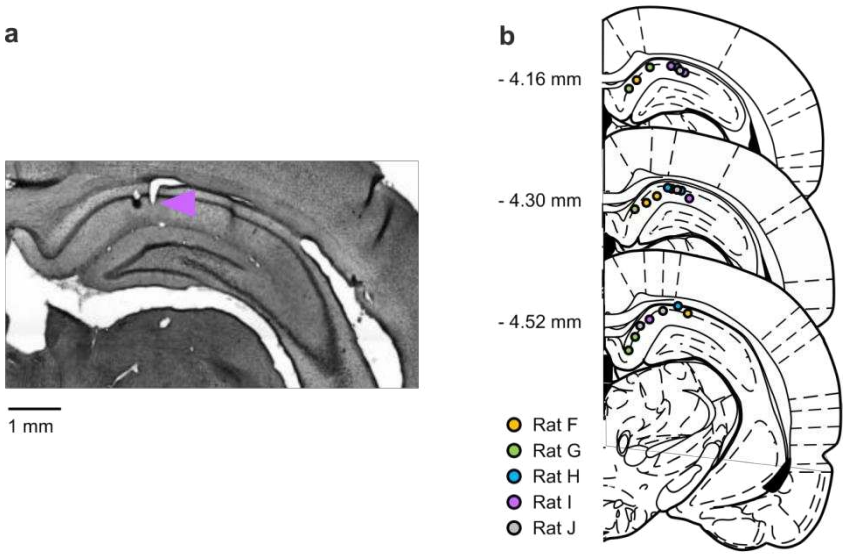

Supplementary Fig. 1 | **Histology.** (a) Coronal section showing histological confirmation of the tetrode placement (lesion site marked with arrowhead) in the CA1 of one rat; (b) Dorsal CA1 tetrode placement for all recorded rats.

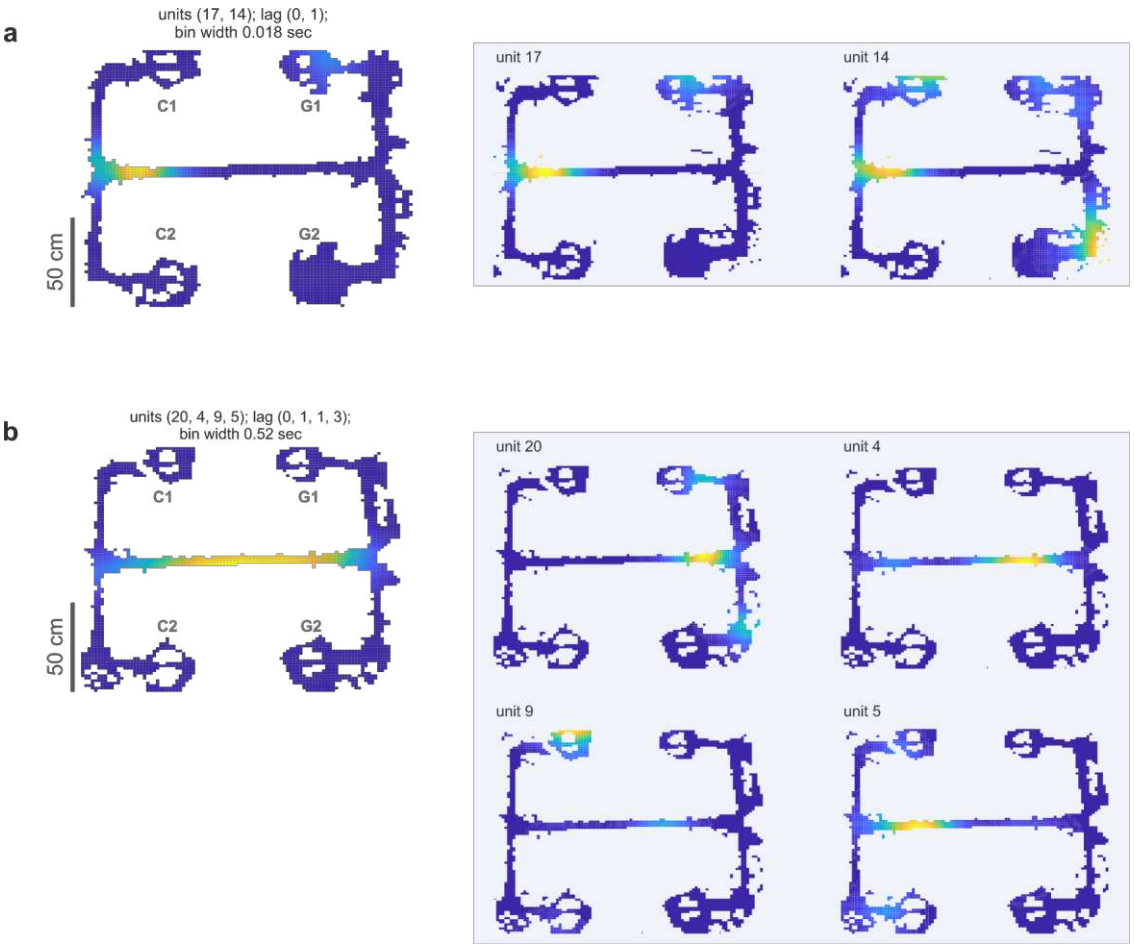

Supplementary Fig. 2 | Place field of assemblies and their composing units. Example of place fields of a spike- (a) and a rate- (b) assembly and of its composing units. While single units fired in multiple place fields throughout the maze, assembly activations were more selective.

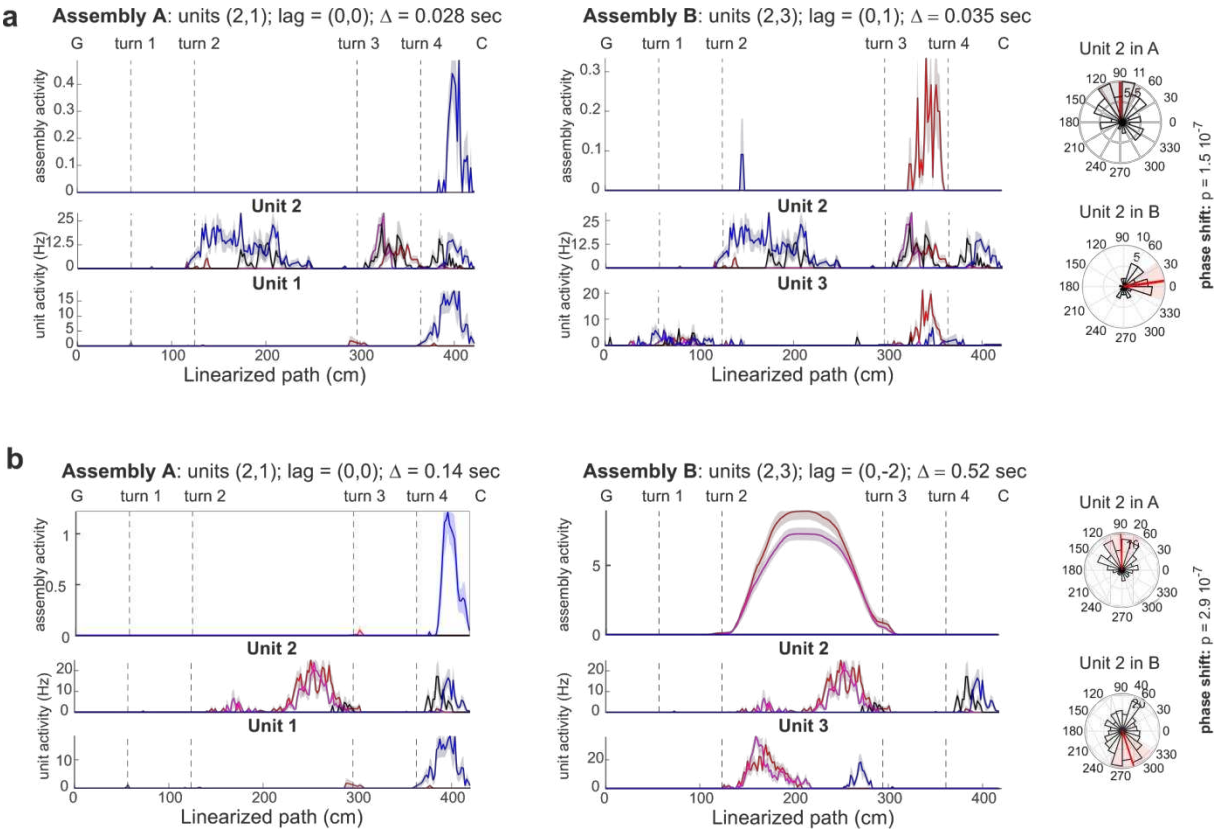

Supplementary Fig. 3 | Changes in unit information coding when joining different assemblies. (a, b). Same as **Fig. 3c**, two additional examples of units with changing phase preference when active in different assemblies.

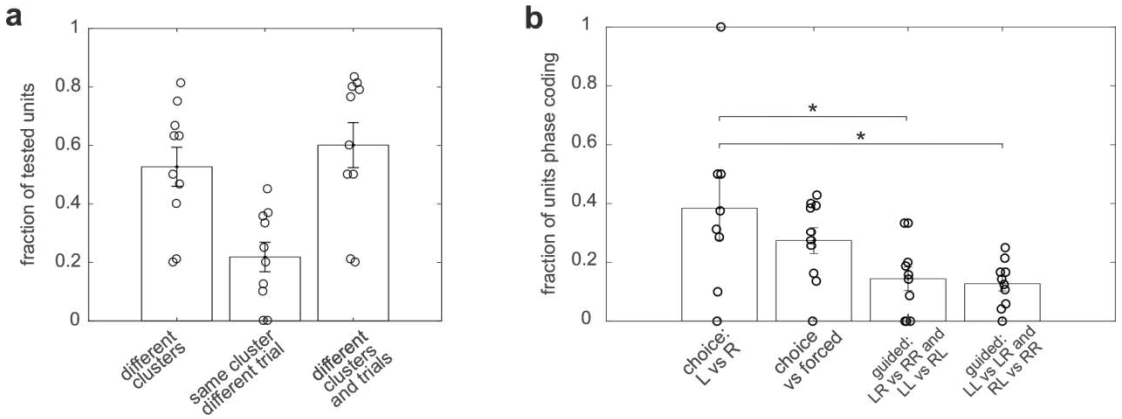

Supplementary Fig. 4 | Phase coding of task-related information. (a, b) Same as **Fig. 5b and d**, respectively, but with analysis performed on spikes fired in epochs of high theta-power. The controls confirm that also when selecting epochs of high theta-power CA1 units result changing phase preference to encode spatial (a) and episodic (b) information (on b, one-way ANOVA, $F(3,34) = 4.3$, $p = .01$; significant Tukey post-hoc comparisons indicated with respect to the figure columns: (I column, II column) $p = 0.03$, (I column, IV column) $= 0.02$).

Parameter	Value
C	250 pF
g_L	10 nS
E_L	-58 mV
Δ_T	2 mV
V_T	-50 mV
E_e	0 mV
E_i	-75 mV
τ_w	120 ms
a	2 nS
b	0.1 nA
V_r	-46 mV
V_s	20 mV

Supplementary Table 1 | Parameters of the adaptive exponential integrate-and-fire model. Parameters used to produce the results presented in **Fig. 6f**.